

Optimal Phase-Control Strategy for Damped-Driven Duffing Oscillators

R. Meucci,^{1,2,3} S. Euzzor,¹ E. Pugliese,^{1,4} S. Zambrano,⁵ M. R. Gallas,^{1,2,3} and J. A. C. Gallas^{1,2,3}

¹*Istituto Nazionale di Ottica, Consiglio Nazionale delle Ricerche, Largo E. Fermi 6, Firenze, Italy*

²*Departamento de Física, Universidade Federal da Paraíba, 58051-970 João Pessoa, Brazil*

³*Instituto de Altos Estudos da Paraíba, Rua Infante Dom Henrique 100-1801, 58039-150 João Pessoa, Brazil*

⁴*Dipartimento di Scienze della Terra, Università degli Studi di Firenze, Via G. La Pira 4, Firenze, Italy*

⁵*Università Vita-Salute San Raffaele, Via Olgettina 58, 20132 Milano, Italy*

(Received 18 September 2015; published 26 January 2016)

Phase-control techniques of chaos aim to extract periodic behaviors from chaotic systems by applying weak harmonic perturbations with a suitably chosen phase. However, little is known about the best strategy for selecting adequate perturbations to reach desired states. Here we use experimental measures and numerical simulations to assess the benefits of controlling individually the three terms of a Duffing oscillator. Using a real-time analog indicator able to discriminate on-the-fly periodic behaviors from chaos, we reconstruct experimentally the phase versus perturbation strength stability areas when periodic perturbations are applied to different terms governing the oscillator. We verify the system to be more sensitive to perturbations applied to the quadratic term of the double-well Duffing oscillator and to the quartic term of the single-well Duffing oscillator.

DOI: 10.1103/PhysRevLett.116.044101

Introduction.—Since the seminal observation of chaos, the Duffing oscillator has played a key role in nonlinear dynamics [1–6]. These pioneering studies considered the motion of a periodically forced steel beam deflected towards two magnets. As is known, the Duffing oscillator [7] is the first system where chaos was observed experimentally in a controlled way, in 1960–1961 by Ueda [4,5]. Duffing-like proxys have been found recently to have the distinctive technological advantage of bypassing noisy spectra which normally pollute driven (i.e., nonautonomous) oscillators [8]. Such oscillators are among the most precise devices presently in existence, allowing its oscillation modes to be measured with very high accuracy. Nowadays, the Duffing oscillator has become a paradigmatic system for the assessment of chaos and for testing analytical methods such as the Melnikov criterion to detect global homoclinic bifurcations [9].

The Duffing oscillator is important in the context of chaos control [10], where the aim is to extract periodic behaviors from chaos by applying small perturbations. In particular, the Duffing oscillator was considered as a paradigmatic system on which it is possible to obtain suppression of chaos by adding a second small harmonic perturbation on the cubic term of the force [11]. The effectiveness of this control method was further tested on an analog implementation of the Duffing oscillator [12], showing the key role played by the phase difference between the applied perturbation and the driving term. The validity of this *phase control of chaos* strategy has been demonstrated in different systems [13–19]. The technique was successfully used to control escaping dynamics in an open system [20,21], and spiking dynamics in an excitable

neuron model system [22]. More recently, phase control has been applied to manipulate entanglement in quantum parametric oscillators by adjusting the amplitude and phase of an external controller applied to a classical counterpart of the quantum system [23].

In spite of the attention drawn by this technique in recent years and its variety of potential applications, several aspects remain unclear. For example, when considering the paradigmatic single- and double-well Duffing oscillators, phase control can be applied either to the two terms deriving from the potential as a parametric perturbation, or to the external drive, as an additive perturbation. However, the size of the stability regions and their sensitivities to each individual perturbation are not known *a priori*. Since the effects of these perturbations differ, their comparison will highlight the differences in perturbing a chaotic trajectory affected by the presence of three fixed points, that is, an unstable saddle point at the origin (0,0) and two stable foci (−1, 0) and (1,0) in the case of a double well, and a single stable fixed point (0,0) for the single well. In this Letter we characterize the effect of these different types of controlling perturbations in an analog implementation of both Duffing oscillators allowing the possibility to discriminate between stable and unstable solutions. We find that the numerical analysis based on the isospike technique [24–26] allows efficient detection and separation between periodic and chaotic orbits visited during the temporal evolution.

Experimental evidence of phase control.—Phase control is first tested in the laboratory by implementing an analog version of driven Duffing oscillator (for the electronic layout of the circuit, see Fig. 1 of the Supplemental Material [27]). The key elements are integrators (Linear

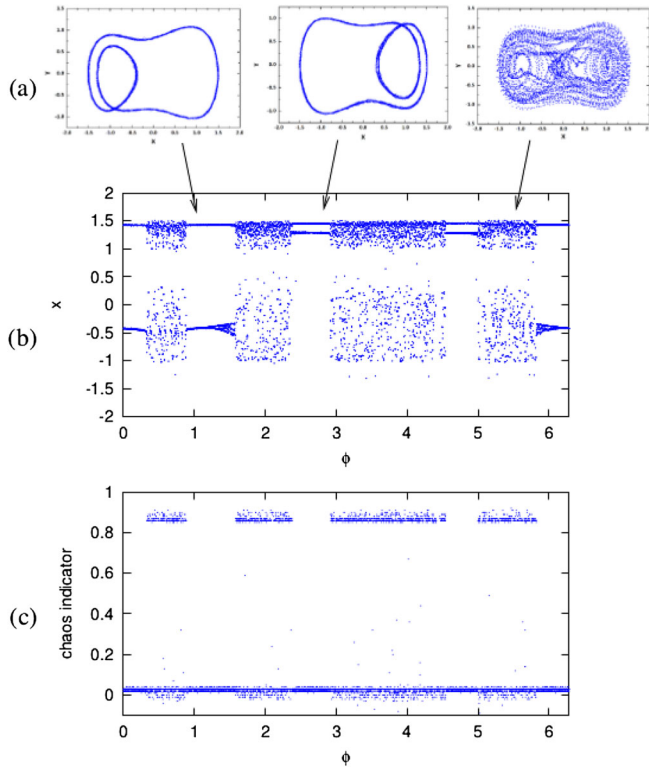


FIG. 1. (a) Examples of regular (left and middle panels) and chaotic orbits (right panel) obtained in our experimental implementation of phase control to the linear term of the oscillator, Eq. (2). (b) Bifurcation diagram from a Poincaré section on the x signal vs phase. (c) Chaos indicator vs phase: we can see that it reproduces the areas of periodicity (chaos indicator close to zero) and of chaos (values between zero and one). Here $\varepsilon = 0.0121$ and $m = 1$.

Technology LT114) and multipliers (Analog Devices MLT04). Two sinusoidal function generators provide the driving signal necessary to lead the system in a chaotic condition and the control signal with an adjustable phase difference with the driving signal, to weakly perturb it. The unperturbed circuit is governed by the equation

$$\gamma^{-2}\ddot{x} + b\gamma^{-1}\dot{x} - x + x^3 = A \cos(2\pi f_d t) \quad (1)$$

where $\gamma = 1/RC$ with $R = 10 \text{ k}\Omega$, $C = 10 \text{ nF}$, A is the driving signal amplitude at $f_d = 1.591 \text{ kHz}$, and $b = 0.25$. Then chaotic oscillations exist in the range $0.438 \leq A \leq 0.442$. To control the oscillator we use the driving term

$$f(t) \equiv 1 + \varepsilon \cos(2\pi f_c t)$$

where ε is the strength of perturbation with frequency f_c . Since the phase difference between the forcing and the control signals is the key parameter of our control strategy, we define $f_c = mf_d + 1/T_{\text{sw}}$ where m can assume the values $1/3, 1/2, 1, 2, 3$ and T_{sw} is the sweeping phase period during which a phase variation of 2π occurs. With

this, may write $f(t) = 1 + \varepsilon \cos[2\pi mf_d t + \phi(t)]$, where $\phi(t) = 2\pi t/T_{\text{sw}}$ and T_{sw} chosen equal to $4s$. Phase control of chaos is then implemented in three distinct ways, acting either as a perturbation to the linear, cubic, or driving term:

$$\gamma^{-2}\ddot{x} + b\gamma^{-1}\dot{x} - f(t)x + x^3 = A \cos(2\pi f_d t) \quad (2)$$

$$\gamma^{-2}\ddot{x} + b\gamma^{-1}\dot{x} - x + f(t)x^3 = A \cos(2\pi f_d t) \quad (3)$$

$$\gamma^{-2}\ddot{x} + b\gamma^{-1}\dot{x} - x + x^3 = f(t)A \cos(2\pi f_d t). \quad (4)$$

In Fig. 1(a) we show experimental representations of the attractors that can be obtained for different values of the phase, either periodic (with one or two loops around the left and the right potential wells) or chaotic. Using the slow sweeping phase technique described above, it is possible to obtain the Poincaré section of the x signal by recording the maxima from its temporal evolution for approximately constant values of the phase difference. Each of these signals, recorded with a Tektronix digital scope TDS7104, consists of 5×10^5 samples for a duration of 4 s during which a phase sweep of 2π occurs. In Fig. 1(b) we show the experimentally obtained bifurcation diagram. Periodic windows are clearly distinguished from chaotic ones during a phase sweep.

In addition to the separation of chaos and regularity using Poincaré sections [Fig. 1(b)], a further discrimination between them is provided by a real time indicator implementing the following on-the-fly algorithm: a low pass filter is applied to the $x^2 + y^2$ signal, and its output is fed to a voltage comparator whose threshold can be adjusted in a suitable way. When the solutions are periodic, the filtered signal converges to its mean value with small periodic oscillations and is easily discriminated from the chaotic regions where the average of the filtered signal is time varying around a lower value due its higher content of harmonics. In our configuration, the indicator assumes zero values when the solutions are stable and a nonzero value when *chaotic*. Such an indicator is plotted as a function of the phase in Fig. 1(c). The indicator is not able to distinguish different periodic attractors as the Poincaré section does but, on the other hand, is able to detect if a periodic orbit is observed in the considered range. Notice that making use of this indicator one could transform the phase control method into a closed loop method, as the OGY control method [10]. Indeed, the phase sweeping could be stopped at a given value based on the values assumed by the indicator, allowing the permanent stabilization of a periodic solution.

An additional advantage of our chaos indicator is that it allows us to obtain, in a straightforward way, the stability regions for our control scheme in the $\varepsilon - \phi$ parameter plane. A reconstruction of such stability regions for the three aforementioned control schemes is reported in Fig. 2, when the perturbation is applied to the linear term x , to the

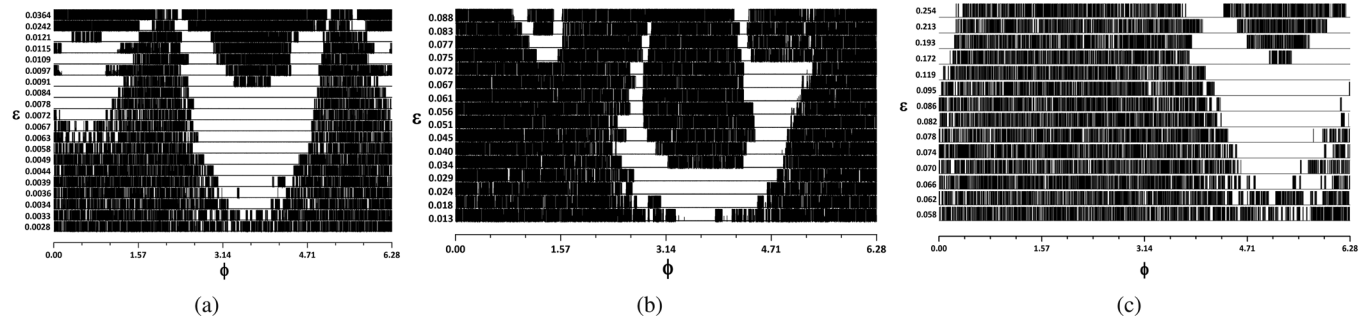


FIG. 2. Experimental reconstruction of the stability regions for the three perturbations considered: (a) control on x ; (b) on x^3 ; (c) on the driving term. White regions represent periodicity domains, black regions represent chaotic domains. Here $m = 1$.

cubic term x^3 , and to the driving term, respectively. We clearly see that the indicator can isolate even small regions, where period-two solutions are entrained. In other terms, we are able to capture fine structures in parameter space of stable solutions embedded in chaos.

As we said, our setup allows us to provide a fast characterization of the dynamics of the system for each value of the phase and the amplitude of the system considered. To obtain a more global view of the effect of each of these perturbations, we evaluated the sensitivity, as the minimum value of ε corresponding to the appropriate phase ϕ , for different values of the ratio m between the frequency of the perturbation and the main driving. The result is shown in Fig. 3.

It appears that the maximum sensitivity is near the resonance value $m = 2$ and when the phased perturbations are applied on the linear term x , rather than on the cubic term or the driving. The reasons can be explained comparing the double- and the single-well oscillators. In the double well, the chaotic attractor is strongly influenced by the unstable saddle at the origin and confined between the two potential valleys around ± 1 . In contrast, in the single well the fixed point at the origin is stable and chaos is reached for high values of the driving term. Then, the chaotic attractor visits areas with x and y values greater than ± 1 (see Fig. 2(a) in the Supplemental Material [27]), implying that the system is more sensitive to perturbation on the cubic term of force. Furthermore, the two chaotic attractors differ in their power spectra due to the different content of even and odd harmonics. The last ones are a consequence of a symmetry breaking occurring in the single-well Duffing oscillator [21,28,29]. As a result, the double well Duffing oscillator is more sensitive when $m = 2$. As far as phased perturbations are applied to the driving term, we observe the single-well to be more sensitive than the double well because for it chaos is reached for much higher values of the driving. Overall, our systematic analysis confirms that an adequate selection of the parameter on which to apply the perturbation is fundamental for the phase control scheme. However, in more complex systems like, e.g., chaotic lasers [30–32], the perturbation might need to be applied distinctly than here.

Numerical simulations.—For comparison, we computed two types of stability diagrams: (i) standard diagrams based on Lyapunov exponents, and (ii) isospike diagrams [24–26], a more fruitful type of diagrams, based on computing the number of local maxima per period for the periodic oscillations. To produce such diagrams, a parameter window of interest is covered with a mesh of $N \times N$ equidistant points. For each point, the temporal evolution is obtained by numerically integrating the oscillators during 10^5 equal steps $h = 0.01$ using the standard fourth-order Runge-Kutta algorithm. In Fig. 4, parameters were scanned horizontally from left to right, starting from $(x, y, t) = (0, 0, 0)$ and proceeding horizontally to the right be “following the attractor”; i.e., instead of systematically reinitializing from $(0,0,0)$, we simply reused the condition already present in the computer buffer from the previous calculation. To compute the number of local maxima per period, after determining the Lyapunov exponents we continued the integration for an additional 10^5 time steps recording up to 800 extrema (maxima and minima) of the variable of interest and checking whether pulses repeated or not. To represent maxima, we use a palette of 17 colors, as

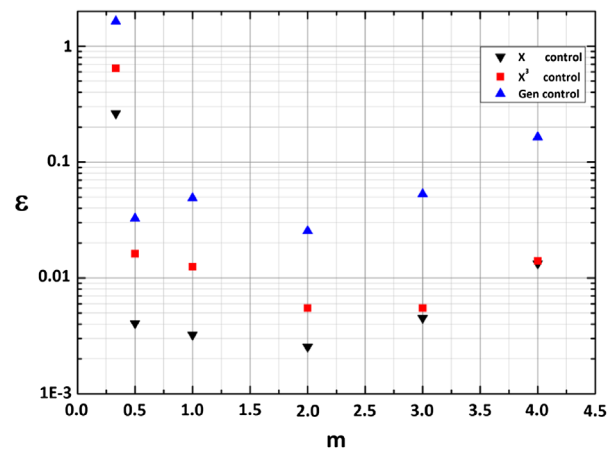


FIG. 3. Relative effectiveness of the ε vs m phase control applied to the x term (\blacktriangledown), on the x^3 term (\blacksquare) and on the driving term (\blacktriangle).

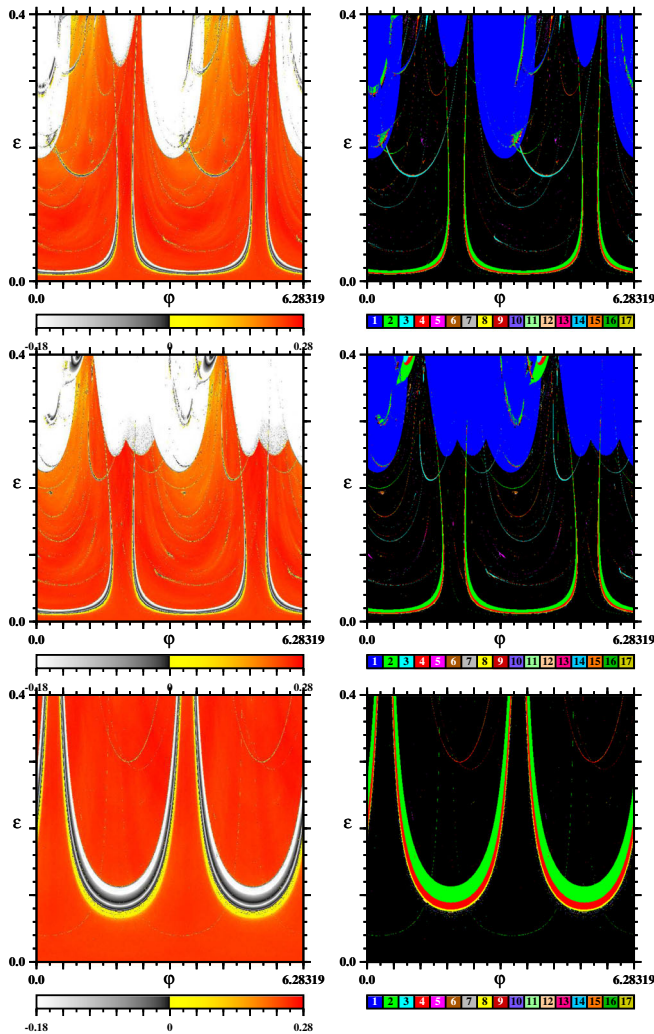


FIG. 4. Stability phases predicted by Eqs. (2)–(4). Lyapunov exponents (left panels) and isospike diagrams [24] (right panels) obtained for control applied on the x term, on the x^3 term, and on the driving term (top to bottom panels, respectively). Here $m = 1$. Each panel shows 600×600 parameter points; i.e., altogether they record the analysis of more than 2.1 million points.

indicated by the color bars in the figures. Patterns with more than 17 maxima are plotted by recycling the 17 basic colors modulo 17. The leftmost panel of Fig. 4 shows a standard Lyapunov stability diagram for the driven Duffing oscillator with the parametric perturbation applied to the x term. In this diagram, gray shadings represent periodic oscillations (negative exponents) while colors denote chaos (positive exponents). From the figures we can observe that there are small differences in perturbing chaos using parametric perturbation on the potential function. Periodic solutions emerge in regular parabolic structures with regions where the phase is ineffective up to ϵ around 0.2 and 0.3, respectively. Increasing further ϵ the organization of periodic or chaotic solutions becomes more and more complex due to parametric perturbation. The

first two figures, as in the experimental case, display fine structures where periodic solutions are entrained for small ranges of the phase. When perturbations are applied to the driving term, periodic solutions appear in the larger domains but their value is greater with respect to parametric ones.

Conclusions.—We investigated the effectiveness of the phase control technique on realistic prototypical systems experimentally and numerically, and discovered an optimal strategy to suppress nonautonomous chaos. We found the phase control to be much more sensitive when applied to the linear forcing term in the double-well potential and at the second harmonic of the driving frequency. With these judicious choices, one can greatly reduce the amplitude of the control forcing and successfully achieve effective control of chaos. It is important to note that, based on the information of the real-time indicator, a desired oscillatory behavior could be stabilized by locking the phase with an additional feedback loop. Such locking could be the core of an efficient feedback control, after a learning period necessary to explore the accessible dynamics. Simulations using the isospike technique confirmed our experiments, further revealing the existence of unanticipated structural complexities in the control parameter space when the perturbations become strong. Now, an enticing open question is to determine how our optimized control performs when the frequency of the drive and the control are not locked at integer multiples or submultiple values of m . In such a case, one needs to deal with quasiperiodic motions and their bifurcations which is a considerably more complicated scenario.

We thank Professor F. T. Arecchi for many helpful discussions. S. Z. thanks the Intra-European Fellowships for career development, Grant No. 2011-298447NonLinKB. M. R. G. and J. A. C. G. thank CNPq, Brazil for support. Bitmaps were computed at the CESUP-UFRGS clusters.

- [1] I. Kovacic and M. J. Brennan, *The Duffing Equation, Nonlinear Oscillators and their Behavior* (Wiley, Chichester, 2011).
- [2] J. Argyris, G. Faust, M. Haase, and R. Friedrich, *An Exploration of Dynamical Systems and Chaos*, 2nd ed. (Springer, New York, 2015).
- [3] S. Strogatz, *Nonlinear Dynamics and Chaos with Applications to Physics, Biology, Chemistry, and Engineering*, 2nd ed. (Westview Press, Boulder, 2015).
- [4] Y. Ueda, *The Road to Chaos* (Aerial Press, Santa Cruz, 1992).
- [5] C. Letellier, *Chaos in Nature* (World Scientific, Singapore, 2013).
- [6] T. Puu, *Attractors, Bifurcations and Chaos, Nonlinear Phenomena in Economics* (Springer, Berlin, 2003).
- [7] When not stated otherwise, our discussions refer to the *double-well* Duffing oscillator of Eq. (1).

- [8] A. Sack, J. G. Freire, E. Lindberg, T. Pöschel, and J. A. C. Gallas, Discontinuous spirals of stable periodic oscillations, *Sci. Rep.* **3**, 3350 (2013).
- [9] R. Chacon, *Control of Homoclinic Chaos by Weak Periodic Perturbations* (World Scientific, Singapore, 2005).
- [10] *Handbook of Chaos Control*, edited by E. Schöll and H. G. Schuster, 2nd ed. (Wiley, Weinheim, 2008).
- [11] R. Lima and M. Pettini, Suppression of chaos by resonant parametric perturbations, *Phys. Rev. A* **41**, 726 (1990).
- [12] S. Zambrano, E. Allaria, S. Brugioni, I. Leyva, R. Meucci, M. A. F. Sanjuán, and F. T. Arecchi, Numerical and experimental exploration of phase control of chaos, *Chaos* **16**, 013111 (2006).
- [13] R. Meucci, W. Gadamski, M. Ciofini, and F. T. Arecchi, Experimental control of chaos by means of weak parametric perturbations, *Phys. Rev. E* **49**, R2528 (1994).
- [14] Z. Qu, G. Hu, G. Yang, and G. Qin, Phase Effect in Taming Nonautonomous Chaos by Weak Harmonic Perturbations, *Phys. Rev. Lett.* **74**, 1736 (1995).
- [15] J. Yang, Z. Qu, and G. Hu, Duffing equation with two periodic forcings: The phase effect, *Phys. Rev. E* **53**, 4402 (1996).
- [16] R. Chacon, Suppression of chaos by selective parametric perturbations, *Phys. Rev. E* **51**, 761 (1995).
- [17] R. Chacon, Role of ultrasubharmonic resonances in taming chaos, *Europhys. Lett.* **54**, 148 (2001).
- [18] H. Cao, X. Chi, and G. Chen, Suppressing or inducing chaos by weak resonant excitations, *Int. J. Bifurcation Chaos Appl. Sci. Eng.* **14**, 1115 (2004).
- [19] A. Y. T. Leung and L. Zengrong, Suppressing chaos for some nonlinear oscillators, *Int. J. Bifurcation Chaos Appl. Sci. Eng.* **14**, 1455 (2004).
- [20] J. M. Seoane, S. Zambrano, S. Euzzor, R. Meucci, F. T. Arecchi, and M. A. F. Sanjuán, Avoiding escapes in open dynamical systems using phase control, *Phys. Rev. E* **78**, 016205 (2008).
- [21] R. Chacon, A. Martínez García-Hoz, J. J. Miralles, and P. J. Martínez, Amplitude modulation control of escape from a potential well, *Phys. Lett. A* **378**, 1104 (2014).
- [22] S. Zambrano, J. M. Seoane, I. P. Mariño, M. A. F. Sanjuán, S. Euzzor, R. Meucci, and F. T. Arecchi, Phase control of excitable systems, *New J. Phys.* **10**, 073030 (2008).
- [23] J. C. Gonzalez-Henao, E. Pugliese, S. Euzzor, S. F. Abdalah, R. Meucci, and J. A. Roversi, Generation of entanglement in quantum parametric oscillators using phase control, *Sci. Rep.* **5**, 13152 (2015).
- [24] J. G. Freire and J. A. C. Gallas, Stern-Brocot trees in the periodicity of mixed-mode oscillations, *Phys. Chem. Chem. Phys.* **13**, 12191 (2011).
- [25] E. Pugliese, R. Meucci, S. Euzzor, J. G. Freire, and J. A. C. Gallas, Complex dynamics of a dc glow discharge tube, *Sci. Rep.* **5**, 8447 (2015).
- [26] L. Junges and J. A. C. Gallas, Stability charts for continuous wide-range control of two mutually delay-coupled semiconductor lasers, *New J. Phys.* **17**, 053038 (2015).
- [27] See Supplemental Material at <http://link.aps.org/supplemental/10.1103/PhysRevLett.116.044101> for a description of the circuit and results for the single-well oscillator.
- [28] V. Englisch, U. Parlitz, and W. Lauterborn, Comparison of winding-number sequences for symmetric and asymmetric oscillatory systems, *Phys. Rev. E* **92**, 022907 (2015).
- [29] U. Parlitz, Common dynamical features of periodically driven strictly dissipative oscillators, *Int. J. Bifurcation Chaos Appl. Sci. Eng.* **03**, 703 (1993).
- [30] S. Zambrano, I. P. Mariño, F. Salvadori, R. Meucci, M. A. F. Sanjuán, and F. T. Arecchi, Phase control of intermittency in dynamical systems, *Phys. Rev. E* **74**, 016202 (2006).
- [31] V. N. Chizhevsky and R. Corbalan, Experimental observation of perturbation-induced intermittency in the dynamics of a loss-modulated CO₂ laser, *Phys. Rev. E* **54**, 4576 (1996).
- [32] V. N. Chizhevsky, R. Vilaseca, and R. Corbalan, Experimental switching in bistability domains induced by resonant perturbations, *Int. J. Bifurcation Chaos Appl. Sci. Eng.* **08**, 1777 (1998).